Structural insights into phosphoinositide 3-kinase activation by the influenza A virus NS1 protein

Benjamin G. Hale[a,1,3], Philip S. Kerry[a,b,1], David Jackson[a], Bernard L. Precious[a], Alexander Gray[c], Marian J. Killip[a], Richard E. Randall[a,b,2], and Rupert J. Russell[a,b,2]

[a]Biomedical Science Research Complex, University of St. Andrews, North Haugh, St. Andrews, Fife, KY16 9ST, United Kingdom; [b]Interdisciplinary Centre for Human and Avian Influenza Research, University of St. Andrews, North Haugh, St. Andrews, Fife, KY16 9ST, United Kingdom; and [c]Division of Molecular Physiology, Faculty of Life Sciences, University of Dundee, Dundee, Tayside, DD1 5EH, United Kingdom

Edited by Robert A. Lamb, Northwestern University, Evanston, IL, and approved December 8, 2009 (received for review September 17, 2009)

Seasonal epidemics and periodic worldwide pandemics caused by influenza A viruses are of continuous concern. The viral nonstructural (NS1) protein is a multifunctional virulence factor that antagonizes several host innate immune defenses during infection. NS1 also directly stimulates class IA phosphoinositide 3-kinase (PI3K) signaling, an essential cell survival pathway commonly mutated in human cancers. Here, we present a 2.3-Å resolution crystal structure of the NS1 effector domain in complex with the inter-SH2 (coiled-coil) domain of p85β, a regulatory subunit of PI3K. Our data emphasize the remarkable isoform specificity of this interaction, and provide insights into the mechanism by which NS1 activates the PI3K (p85β:p110) holoenzyme. A model of the NS1:PI3K heterotrimeric complex reveals that NS1 uses the coiled-coil as a structural tether to sterically prevent normal inhibitory contacts between the N-terminal SH2 domain of p85β and the p110 catalytic subunit. Furthermore, in this model, NS1 makes extensive contacts with the C2/kinase domains of p110, and a small acidic α-helix of NS1 sits adjacent to the highly basic activation loop of the enzyme. During infection, a recombinant influenza A virus expressing NS1 with charge-disruption mutations in this acidic α-helix is unable to stimulate the production of phosphatidylinositol 3,4,5-trisphosphate or the phosphorylation of Akt. Despite this, the charge-disruption mutations in NS1 do not affect its ability to interact with the p85β inter-SH2 domain in vitro. Overall, these data suggest that both direct binding of NS1 to p85β (resulting in repositioning of the N-terminal SH2 domain) and possible NS1:p110 contacts contribute to PI3K activation.

activation loop | coiled-coil | crystallography | PI3-kinase

Class IA phosphoinositide 3-kinases (PI3Ks) are obligate heterodimeric enzymes consisting of a 110-kDa catalytic subunit (p110α, p110β, or p110δ) bound to a noncatalytic 85-kDa regulatory subunit (typically p85α or p85β) (1). Growth factor receptor-mediated activation of PI3K requires the relocalization of p85:p110 heterodimers to the plasma membrane, where disinhibition of p110 by p85 leads to the production of phosphatidylinositol 3,4,5-trisphosphate (PIP_3). PIP_3 is an intracellular lipid second messenger that recruits pleckstrin homology domain-containing effectors (including protein kinases such as Akt) to the membrane. Subsequent activation of these effectors stimulates a plethora of signaling cascades that regulate diverse biological processes, including cell survival, proliferation, and metabolism (2). Given that PI3K is among the most frequently mutated enzymes associated with human cancers (3, 4), there is considerable interest in trying to understand the structural basis for both normal and pathophysiological regulation of p110 by p85 (5–7). Such studies are likely to yield insights into the novel mechanisms by which PI3K can be aberrantly activated, and may provide the focus for designing selective inhibitors targeting specific diseases.

During infection, the PI3K signaling pathway is activated by influenza A viruses in order to promote efficient virus replication (8). Specifically, the multifunctional viral nonstructural (NS1) protein binds directly to p85β, but not p85α, and stimulates the lipid kinase activity of p85β-associated p110 (8–10). The full biological consequences of NS1-mediated PI3K activation are far from clear, although an association with regulating lung epithelium ion channel activity has been proposed (11). Early studies also suggested that NS1-activated PI3K contributes to the suppression of cellular apoptosis during virus infection (12–15), but very recent data now indicate that this may not be the case (16). Thus, the precise role of this important signaling pathway with respect to the influenza A virus replication cycle has yet to be firmly established.

The p85β regulatory subunit is made up of five domains: an N-terminal SH3 domain, a GTP-ase activating protein domain, and two SH2 domains (termed nSH2 and cSH2), which flank the inter-SH2 (β-iSH2) domain. NS1 consists of an N-terminal RNA-binding domain (RBD) flexibly linked to a C-terminal effector domain (ED) (10, 17). We have previously shown that β-iSH2 (a rigid coiled-coil scaffold for the p110 subunit) (5, 6) is the primary direct binding site for the NS1 ED (18). Here, in order to gain further insights into how NS1 might modify normal intermolecular and intramolecular regulatory contacts within the p85β:p110 holoenzyme, we purified and crystallized the ED:β-iSH2 complex. Our data reveal the molecular basis for p85 isoform discrimination by NS1, and confirm the location of NS1 residues Tyr89 (8) and Pro164 (14) at the binding interface with p85β. We also generated a model of the NS1:PI3K heterotrimeric complex, and propose that NS1 acts by physically blocking normal inhibitory contacts between the p85β nSH2 domain and p110. In addition, we found that charged residues within a small, acidic α-helix of NS1 are also required for stimulating PI3K activity during infection, possibly by interacting directly with p110. Intriguingly, these same charged residues of NS1 have previously been implicated in limiting interferon (IFN) production (19). Using genetically engineered recombinant influenza A viruses, we demonstrate functional overlap between two NS1 activities by showing that this small α-helix of NS1 plays independent roles in affecting both PI3K activation and IFN-antagonism.

Author contributions: B.G.H., P.S.K., D.J., B.L.P., A.G., M.J.K., R.E.R., and R.J.R. designed research; B.G.H., P.S.K., D.J., B.L.P., A.G., M.J.K., and R.J.R. performed research; B.G.H., P.S.K., D.J., B.L.P., A.G., M.J.K., R.E.R., and R.J.R.. analyzed data; and B.G.H., and R.J.R. wrote the paper.

The authors declare no conflict of interest.

This article is a PNAS Direct Submission.

Freely available online through the PNAS open access option.

Data deposition: Coordinates and structure factors for the ED:β-iSH2 complex have been deposited with the Protein Data Bank (accession code 3L4Q).

[1]B.G.H. and P.S.K. contributed equally to this work.

[2]To whom correspondence may be addressed. E-mail: rer@st-andrews.ac.uk or rjmr@st-andrews.ac.uk.

[3]Present address: Department of Microbiology, Mount Sinai School of Medicine, One Gustave L. Levy Place, New York, NY 10029.

This article contains supporting information online at www.pnas.org/cgi/content/full/0910715107/DCSupplemental.

Results and Discussion

The ED:β-iSH2 Complex. The crystal structure of the NS1 ED in complex with the p85β iSH2 (β-iSH2) domain was solved to 2.3-Å resolution by molecular replacement (see Table 1 and Fig. S1). The asymmetric unit reveals a tetrameric complex consisting of the major in-solution homodimeric form of NS1 ED (helix–helix) (20) with one β-iSH2 domain bound on either side (Fig. 1*A*). However, given that the p85 iSH2 domain likely sits in plane with the membrane during PI3K activation (5, 7), such a tetramer would be sterically prohibited in a physiological context (Fig. 1*B*). We therefore believe that the functional biological unit is formed by a single ED interacting with one end of the β-iSH2 coiled-coil. Indeed, dimerization of the NS1 ED is not essential for efficient β-iSH2 binding (Fig. S2), and the NS1 ED has been suggested to adopt multiple different homotypic assemblies depending on its function (17, 20–22). The heterodimeric ED:β-iSH2 structure thus resembles a golf club–shaped complex (Fig. 2*A*). Central to the complex is the formation of a four-helix bundle composed of a short conserved acidic α-helix of NS1 ED (residues 95–100) and all three α-helices of β-iSH2 (Fig. 2*B*). NS1 ED binds to the end of β-iSH2 opposite the major p110 tethering site (5, 6) and encompasses residues 562–589 of p85β. Such positioning of NS1 ED is in full agreement with previous β-iSH2 deletion mapping studies (9, 18). 755 Å^2 of surface area is buried from solvent upon complex formation. As detailed below, possible stabilizing contacts between NS1 and p110 would significantly increase buried surface area in the physiological NS1:PI3K heterotrimeric complex.

Residues at the ED:β-iSH2 Interface. Support for the validity of our structure is gained from prior mutational analyses of NS1 that identified amino-acid substitutions that disrupt complex formation. In particular, previous studies have highlighted the importance of Tyr89 as an essential residue for the binding of NS1 ED to p85β (8). The conservative mutation of this tyrosine to phenylalanine completely abolishes stable complex formation, as well as the activation of PI3K (8). Our structure reveals that Tyr89 is positioned at the heart of the complex and forms a hydrogen bond to Asp569 of β-iSH2 (Fig. 2*C*, stereo image in Fig. S3). Pro164 and Pro167 of NS1 have also been reported to be involved in complex formation (14). Whereas Pro167 is clearly not an interface residue, Pro164 lies at an extreme edge of the interface, effectively closing off the complex (Fig. 2*C*). Both Tyr89 and Pro164 bury more than

Table 1. Data collection and refinement statistics

	ED:β-iSH2
Data collection	
Space group	$P2_12_12_1$
Cell dimensions	
a, *b*, *c* (Å)	57.95, 98.67, 149.94
α, β, γ (°)	90, 90, 90
Resolution (Å)	2.30 (2.42–2.30)*
R_{merge}	8.9 (65.5)
$I/\sigma I$	12.8 (2.6)
Completeness (%)	99.5 (98.7)
Redundancy	4.7
Refinement	
Resolution (Å)	82.42–2.30
No. reflections	36826
R_{work}/R_{free}	23.2/29.2
No. atoms	
Protein	4629
Ligand/ion	12
Water	281
B-factors	
Protein	51.2
rms deviations	
Bond lengths (Å)	0.021
Bond angles (°)	1.84

*Values in parentheses are for highest-resolution shell.

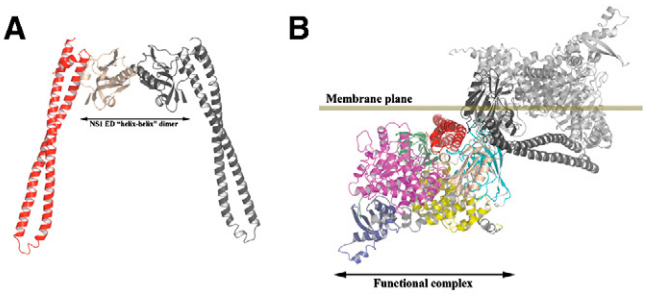

Fig. 1. Physiological constraints suggest that the NS1 ED binds β-iSH2 as a monomer. (*A*) Tetrameric arrangement of the ED:β-iSH2 complex that is observed in the asymmetric unit. Central to the arrangement is an NS1 ED helix–helix dimer that is the predominant multimeric form in solution (20) and is observed in previous ED crystal structures (21, 36). One ED:β-iSH2 complex is colored as in Fig. 2 and the other dark gray. (*B*) Model of how the tetrameric complex would orient with respect to the lipid membrane. One heterodimeric ED:β-iSH2 complex has been orientated in a manner analogous to that proposed for the p85:p110 holocomplex (see Fig. 3*B* in ref. 5) and colored as in Fig. 3. The other heterodimeric complex is colored gray for p110 and dark gray for the ED:β-iSH2 complex. It is apparent from this orientation that a tetrameric ED:β-iSH2 complex is incompatible which the proposed mode of membrane association of PI3K.

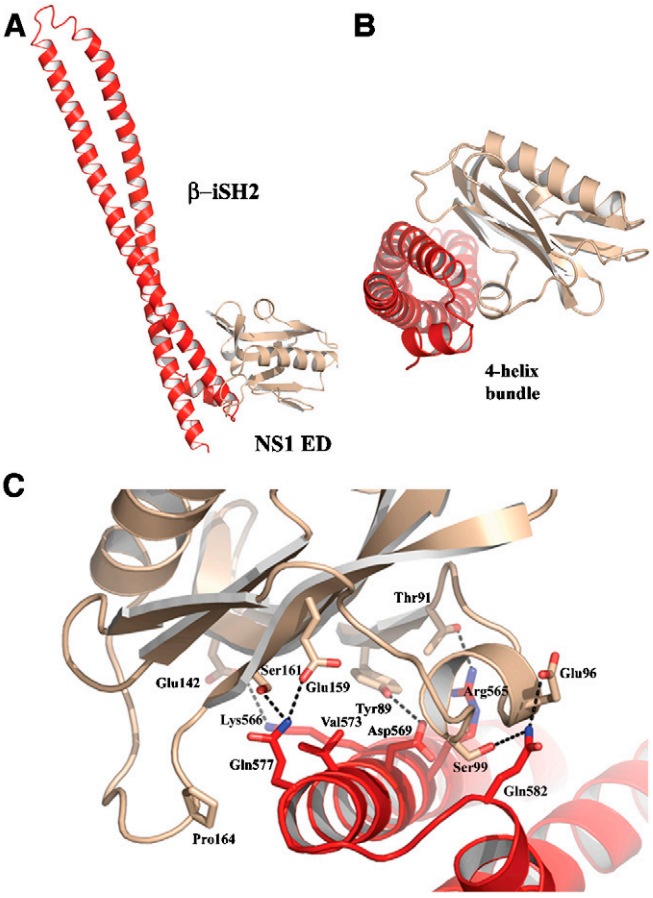

Fig. 2. Structure of the ED:β-iSH2 complex. (*A*) Cartoon representation of the ED:β-iSH2 complex. (*B*) Cartoon representation of the four-helix bundle formed at the complex interface. (*C*) Residues at the ED:β-iSH2 interface. Potential hydrogen bonds are highlighted. Individual residues are shown in stick representation. NS1 ED is colored gold, and β-iSH2 is colored red.

BIOCHEMISTRY

90 Å^2 of surface area upon binding β-iSH2 and represent the two residues of NS1 ED that contribute most to interfacial surface area. In addition, Glu142 of NS1 has been implicated in β-iSH2 binding (9), and inspection of the ED:β-iSH2 complex reveals that this residue may form a salt bridge with Lys566 of β-iSH2 (Fig. 2*C*). Other residues of NS1 ED and β-iSH2 found at the complex interface are shown in Fig. 2*C* and listed in Tables S1 and S2.

Despite high sequence identity between the p85α and p85β iSH2 domains, it is remarkable that NS1 binds only to the p85β, but not p85α, isoform of PI3K (8). Previous mutational studies on β-iSH2 clearly defined Val573 as critically mediating the NS1:p85β interaction (9). Reciprocal gain of function experiments with p85α further demonstrated that mutation of Met582 (the corresponding residue of p85α) to valine allows NS1 to bind this mutant p85α and subsequently stimulate the lipid kinase activity of p85α-associated p110 (9). In the ED:β-iSH2 complex presented here, Val573 lies directly at the interface and buries over 70 Å^2 upon complex formation (Fig. 2*C*). It is clear that a methionine at this position would be sterically precluded, which serves to explain structurally the p85 isoform specificity exhibited by NS1 (8).

Model of the Heterotrimeric NS1:PI3K Complex. To investigate possible mechanisms for NS1-mediated activation of PI3K, we superimposed our ED:β-iSH2 structure onto the reported crystal structure of full-length p110α in complex with p85α iSH2 (5) by aligning the two homologous iSH2 domains (Fig. 3*A*, *Left* panel). The previous p85α iSH2 domain structures have been determined both in the presence and absence of p110α (5–7), and all iSH2 crystal structures to date, including our β-iSH2 structure, are highly similar. Remarkably, there is almost no overlap between the Cα chains of p110α and NS1 ED in our superimposed model, suggesting that both complex structures are compatible with one another, and that a heterotrimeric NS1:p85β:p110 complex can occur physiologically. Indeed, previous biochemical data have shown that NS1 does not displace p110 from p85β, despite binding the β-iSH2 domain (9, 18). These observations further support the idea that our heterotrimeric model is similar to what would be observed with full-length protein complexes in vivo.

In our model, NS1 ED lies sandwiched between the p85β iSH2 domain and the kinase, helical, and C2 domains of p110α (Fig. 3*B*). Although NS1 has been reported not to bind p110 directly (9), it is highly likely that NS1:p110 contacts stabilize the heterotrimeric complex. Intriguingly, many oncogenic mutation "hot spots" within both p85 (3) and p110 (4) that cause constitutively active PI3K phenotypes are located at the proposed interfaces with NS1 (labeled residues in Fig. 3*B*), highlighting the general importance of this region for regulating kinase activity.

Tethering of NS1 to the β-iSH2 Domain Would Prevent nSH2 Interactions with p110. The PI3K holoenzyme is normally held inactive in the cytoplasm, with the p85 nSH2 domain positioned such that it makes inhibitory charge–charge contacts with p110, predominantly via the helical domain (6), but also to a lesser extent with the C2 and kinase domains (5, 7). Extracellular signal-induced phosphotyrosine docking sites compete with the p110 helical domain for nSH2 binding (6, 7), thereby causing both the relocalization of PI3K to the plasma membrane and the disinhibition of p110 lipid kinase activity. This disinhibition is proposed to be a direct consequence of conformational changes in p85 such that the nSH2 domain is no longer positioned correctly in order to inhibit the p110 subunit (6). The recently obtained crystal structure of p110α in an apparent inhibitory complex with both the nSH2 and iSH2 domains of p85α confirms that nSH2 makes contact with multiple domains of p110 (Fig. 3*A*, *Right* panel and Fig. 3*C*) (7). The positioning of NS1 ED in our model structure (Fig. 3*A*, *Left* panel and Fig. 3*B*) shows that NS1 ED sits almost exactly where the p85 nSH2 domain resides in the catalytically inactive p85:p110 complex (5–7). It is currently unknown exactly

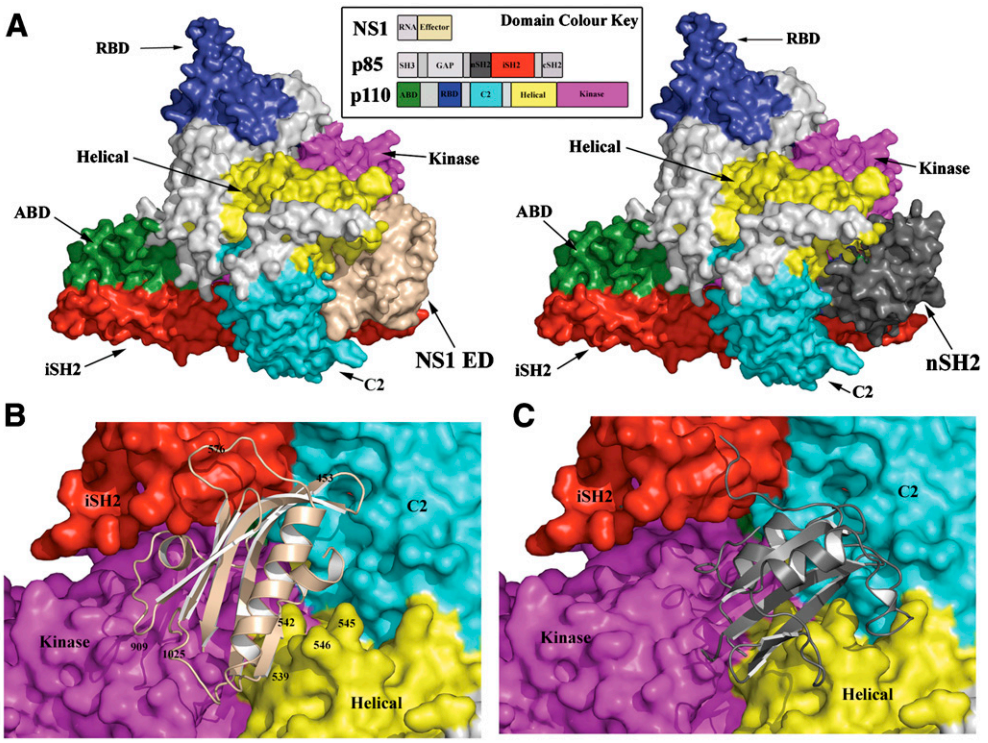

Fig. 3. Model of the NS1:PI3K heterotrimer. (*A*) *Left*. Model of the interaction between NS1 ED and the β-iSH2:p110α complex. *Right*. Structure of a p85α nSH2-iSH2 fragment in complex with p110α as determined by Mandelker et al. (7). Individual domains are colored separately and labeled. Regions linking domains are colored white. (*B*) Close-up view of the NS1 ED location in the modeled heterotrimeric complex. The location of cancer-associated mutations in p85α/p110α that cause constitutive kinase activation are highlighted. (*C*) Close-up view of the nSH2 domain location in the structure by Mandelker et al. (7).

how nSH2 regulates kinase activity by docking next to the p110 helical/kinase domains. However, it is clear that NS1 binding to β-iSH2 would sterically prevent nSH2 from occupying its inhibitory position. This may provide a simple and plausible mechanism by which NS1 mediates activation of p110 kinase activity, and it assumes that the affinity of NS1 for the PI3K holoenzyme is higher than that for the intracomplex interaction between p85β nSH2 and p110.

Residues of NS1 Located at the Contact Interface with the p110 Kinase Domain Are Required for PI3K Activation During Infection. A detailed comparison of the positioning of nSH2 and NS1 ED relative to p110 reveals a number of differences. Firstly, as detailed above, NS1 ED makes extensive contacts with the p85 iSH2 domain, a feature which probably allows NS1 to tether itself to the enzyme and thus displace nSH2 from its charge–charge interactions with p110. Secondly, the nSH2 domain predominantly interacts with the p110 helical domain (Fig. 3*C*), and nSH2 contacts with residues 542, 545, and 546 in p110 have previously been shown to be particularly important for kinase inhibition (6). In our model, NS1 ED does not shield residues 545 and 546 in the helical domain, and instead it appears to make more extensive interactions with the p110 C2 and kinase domains (Fig. 3*B*). Based on this observation, we speculated that, in addition to physically preventing the inhibitory contacts of p85β nSH2 with p110, direct interactions between the NS1 ED and p110 may also influence kinase activity.

The activation loop of p110 (residues 933–957) lies close to the proposed interface of the p110 kinase domain with NS1 ED (Fig. 4*A*). In the published crystal structures of iSH2:p110α complexes, residues 941-950 (KKKKFGYKRE) are disordered (5, 7), possibly reflecting an inactive state of the activation loop. In our model, the small acidic α-helix of NS1 ED that participates in the four-helix bundle of the ED:β-iSH2 complex sits adjacent to this section of the highly basic activation loop, and therefore has the potential to interact with it (Fig. 4*A*). Thus, a possible additional function of the NS1 ED may be to directly modulate p110 activity by manipulating the kinase activation loop. Such an unusual mechanism of regulation is not unprecedented. For example, the LKB1 protein kinase is allosterically activated by other proteins stabilizing its activation loop (23).

We generated a recombinant influenza A virus [Udorn strain (Ud)] that expresses a mutant NS1 protein with charge-disruption mutations in its acidic α-helix (E96A/E97A). Glu96/Glu97 are highly conserved in nearly all strains of influenza A viruses sequenced to date, and reside on the face of the α-helix opposite to that involved in ED:β-iSH2 complex formation (Fig. 2*C*). Strikingly, unlike wild-type virus (rUd WT), the rUd-E96/97A virus was unable to stimulate cellular production of PIP_3 during infection (Fig. 4*B*), and consequently this virus failed to induce Ser473 phosphorylation of Akt (Fig. 4*C*). In influenza A virus infected cells these processes are strictly dependent on NS1 binding a p85β:p110 complex and stimulating p110 kinase activity (8, 9, 18). Such a phenotype was compar-

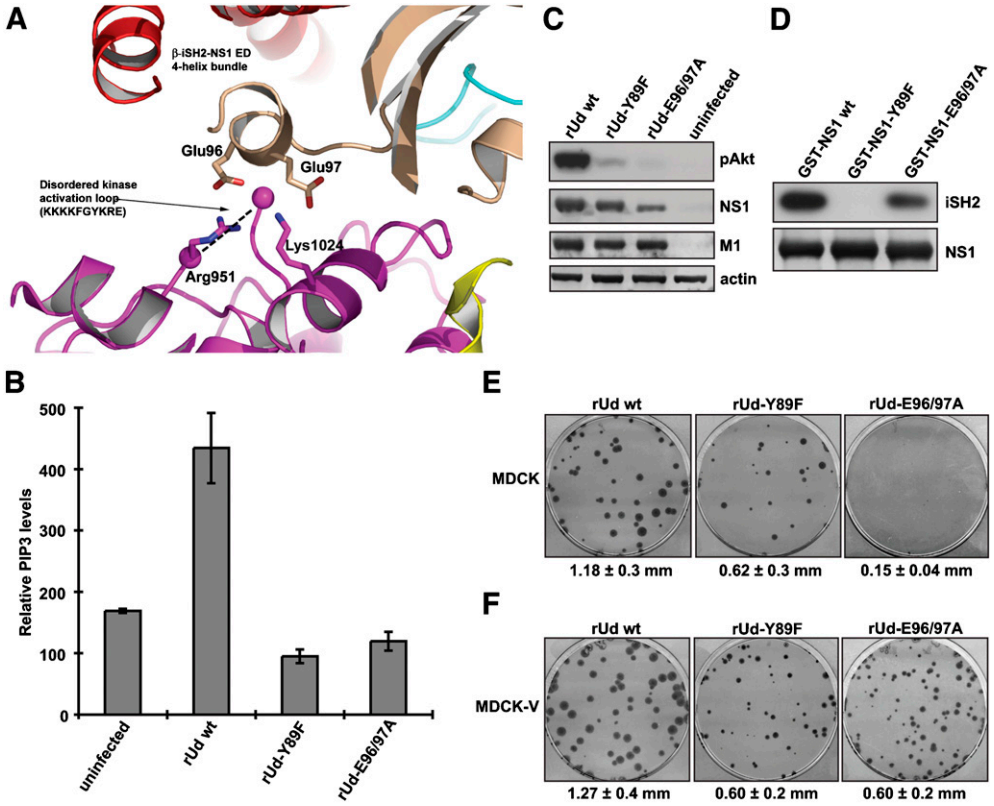

Fig. 4. Roles of the NS1 acidic α-helix in both PI3K activation and IFN-antagonism. (*A*) Potential interaction between the NS1 ED and the p110α kinase activation loop. Domains of p85β, p110α, and NS1 ED are shown in cartoon representation. The edges of the disordered p110α activation loop are highlighted by spheres colored magenta. Specific residues are shown in stick representation. (*B*) The rUd-E96/97A virus does not activate PI3K. 1321N1 cells (which lack the PIP_3 phosphatase, PTEN) (37) were infected with rUd WT, rUd-Y89F, or rUd-E96/97A viruses at an MOI of 5 PFU/cell for 10 h prior to analysis of total PIP_3 levels. Bars show mean values obtained from triplicate samples assayed in duplicate. Error bars represent standard deviation. (*C*) A549 cells were infected as for (*B*). Cells were lysed and proteins analyzed by immunoblotting. The level of PI3K activation was determined by detection of phospho-Akt (Ser473). Viral NS1 and M1 proteins were detected as markers of infection. β-actin was used as a loading control. (*D*) GST-pulldown experiment showing the interaction of NS1 with β-iSH2. GST-NS1 proteins were immobilized onto agarose beads and incubated with 293T cell lysates expressing myc-tagged β-iSH2. NS1:β-iSH2 complexes were separated by SDS-PAGE and detected by immunoblotting using anti-NS1 and anti-myc antibodies. (*E*) Mean plaque size of recombinant rUd WT, rUd-Y89F, and rUd-E96/97A viruses in MDCK cells. Plaques were immunostained 3 days postinfection, and mean plaque size was determined (±SD). (*F*) Mean plaque size of recombinant rUd WT, rUd-Y89F, and rUd-E96/97A viruses in MDCK-V cells (targeted degradation of STAT1) (24). Plaques were immunostained 3 days postinfection, and mean plaque size was determined (±SD).

able to that of the previously reported rUd-Y89F virus (in which NS1 is unable to bind p85β) (8) (Figs. 4*B* and 4*C*). Nevertheless, as expected from our structure, GST-pulldown experiments confirmed that the mutant NS1 protein (E96/97A) still binds the iSH2 domain of p85β (Fig. 4*D*). Thus, although NS1 binding to the β-iSH2 domain will clearly disrupt inhibitory contacts between p85β nSH2 and p110 (6), this may not be fully sufficient for NS1 to activate PI3K. Our data suggest that additional contacts between the small α-helix of NS1 and the p110 kinase domain (possibly via the activation loop) likely contribute to kinase activation in cells.

Residues of the NS1 Acidic α-Helix Have Dual Roles During Infection. The biological consequences of NS1 activating PI3K have yet to be firmly established (16). Given that mutation of Glu96/Glu97 in NS1 has been reported to dramatically reduce NS1's IFN-antagonistic ability (19), we further characterized the rUd-E96/97A virus in order to establish if PI3K activation and IFN antagonism were linked or could be functionally separated. In contrast to the rUd WT and rUd-Y89F viruses, the rUd-E96/97A virus induced large amounts of IFN following infection of A549 cells (Fig. S4*A*). Thus, inability of the rUd-E96/97A virus to activate PI3K alone is unlikely to be the reason why it induces such high amounts of IFN. Furthermore, in IFN-competent Madin–Darby canine kidney (MDCK) cells, the rUd-E96/97A virus produced significantly smaller plaques than WT virus, whereas the rUd-Y89F virus showed an intermediate plaque phenotype (Fig. 4*E*). However, in cells unable to respond to IFN (MDCK-V cells), the mean plaque sizes of rUd-E96/97A and rUd-Y89F viruses were similar, yet still clearly smaller, than those of WT (Fig. 4*F*). Thus, expression of a known IFN-antagonist protein (PIV5 V) (24) can "rescue" the phenotype of the rUd-E96/97A virus with respect to its disabled IFN-antagonist properties, but not its disabled PI3K-activating properties. As the rUd-Y89F virus is only disabled in its PI3K-activating properties (Fig. S4*A*), an IFN antagonist provided *in trans* cannot rescue the phenotype of this virus. Similar results were also obtained in A549 cells using a different IFN-antagonist protein (BVDV NPro) (25) (Fig. S4*B*). We conclude that Glu96/Glu97 are important for the IFN-antagonistic function of NS1 (19), but this is independent of their role in PI3K activation. Glu96/Glu97 therefore appear to be critical for at least two separate NS1 functions.

Concluding Remarks. In this study, we have explored the structural basis for influenza A virus NS1 protein binding to the p85β iSH2 domain. We have also generated a structural model of how this viral protein may activate the PI3K holoenzyme, and used genetically engineered mutant influenza A viruses to try and validate parts of this model in tissue culture. Although NS1 binding to the β-iSH2 domain will clearly disrupt essential inhibitory contacts between p85β and p110 (6), our results suggest that this may be insufficient to activate PI3K. We therefore hypothesize that to fully stimulate kinase activity the acidic α-helix of NS1 also interacts with the p110 activation loop. Such a previously undescribed mechanism may have important implications for understanding the normal regulatory control of PI3K, and it is therefore intriguing to speculate that similar positive regulation of the activation loop occurs physiologically in the absence of viral hijack. This would most likely be regulation by p85 itself, and possibly by the nSH2 domain. Thus, it could be that NS1 ED mimics the positioning of nSH2 during normal extracellular signal-induced PI3K activation. It will clearly be very informative to obtain a structure of the p85:p110 complex in its true biological disinhibited state.

During our structural and biochemical studies we identified a single region on the NS1 protein that mediates two independent and distinct roles: PI3K activation and IFN-antagonism. Such a dual phenomenon has been reported previously for NS1 with respect to its ability to regulate host dsRNA-activated protein kinase activity and viral RNA synthesis (26) and is perhaps not wholly surprising given the plethora of activities attributed to this small (26 kDa) viral protein (10). This highlights the fact that it is very difficult to experimentally knock out specific functions of NS1, a concept we have recently explored using a panel of recombinant mutant NS1 viruses (16). Thus, an intrinsic caveat to our work here is that there may be other properties of NS1 affected by mutating Glu96/Glu97 that we are unaware of, and these may have biased our results. Nevertheless, our structural model should still prove extremely useful in designing further experiments to understand the NS1:PI3K functional interface. Indeed, to formally prove our hypotheses, we believe it will be essential to develop in vitro PI3K activity assays using both purified NS1 and p85β:p110, as well as establish conditions to purify and crystallize the full-length NS1:PI3K heterotrimer.

Other than single regions of NS1 being necessary for more than one role, we speculate that some functions of NS1 will depend upon different multimeric conformations of the protein. This is borne out by our observation that to bind PI3K in a physiological context, the NS1 ED would have to be in a monomeric state (the positioning and state of the NS1 RBD has yet to be determined during PI3K activation). Thus, future studies on the interactions of full-length influenza A virus NS1 protein with all of its host-cell binding partners may underscore both the multifunctional and "multistructural" nature of this important virulence factor.

Materials and Methods

Plasmid Construction and Transfection. cDNA encoding residues 73–230 (ED) from the NS1 protein of influenza virus strain A/Puerto Rico/8/34 (H1N1; PR8) was amplified by PCR and ligated between the EcoRI and NotI sites of a modified pRSFDuet-1 coexpression vector (Novagen). cDNA encoding residues 424–593 of bovine p85β (β-iSH2) (18) was ligated between the NdeI and XhoI sites of the same vector. Four-primer overlap PCR was used to introduce a specific site-directed point mutation into the β-iSH2 construct, resulting in a C495S amino-acid substitution. This was designed to reduce protein aggregation, and is distal to the NS1 binding site. Integrity of the construct was confirmed by DNA sequencing.

The pHH-NS1-E96/97A plasmid used in the reverse genetics system to create the rUd-E96/97A virus was generated by site-directed mutagenesis of pHH-NS using the QuikChange mutagenesis kit (Stratagene) and specific primers (forward 5′-CTGACATGACTATTGCGGCATTGTCAAGGGACTGG-3′ and reverse 5′-CCAGTCCCTTGACAATGCCGCAATAGTCATGTCAG-3′). The sequence of pHH-NS1-E96/97A was confirmed by DNA sequencing prior to use. The pGEX-NS1-E96/97A plasmid for bacterial expression of NS1 was generated using the same site-directed mutagenesis protocol and primers. Expression of myc-tagged β-iSH2 was achieved by transfecting 7×10^6 293T cells with 5 μg of pEF-β-iSH2 (18) using FuGENE 6 transfection reagent (Roche).

Protein Expression and Purification. Recombinant 6His-tagged NS1 ED was coexpressed with untagged β-iSH2 in *Escherichia coli* strain BL-21 (DE3). Induction and purification were performed as previously described (20).

GST-NS1 proteins were expressed in BL-21 (DE3) cells as described above, except that due to the apparent insolubility of the GST-NS1-E96/97A protein, cells were resuspended and lysed in STE buffer [10 mM Tris-HCl (pH 7.8), 200 mM NaCl, 1 mM EDTA] supplemented with 1.5% sarkosyl (27). After sonication, clarified lysates were incubated with immobilized glutathione-agarose beads (Thermo-Fisher) for 1 h at 4 °C, washed in STE, and resuspended in STE as a 50% slurry.

Protein Crystallization, Data Collection, and Structure Solution/Refinement. ED:β-iSH2 complex crystals were obtained by vapor diffusion in hanging drops consisting of 2 μL reservoir solution [0.2 M HEPES (pH 6.5), 0.2 M sodium chloride, 15% PEG 8000, 14% isopropanol] and 2 μL concentrated protein solution (approximately 1.2 mg/mL). The crystals were cryoprotected with reservoir solution supplemented with 20% glycerol, and data were collected on beamline IO3 at the Diamond Light Source at 100 K with a DSC Q315 CCD and processed with Mosflm (28). The asymmetric unit contains two NS1 EDs and two β-iSH2 domains, which corresponds to a solvent content of 62%. The structure was solved by molecular replacement using the program PHASER, an existing PR8/NS1 ED structure, and the iSH2 domain structure of the PI3K iSH2/ABD complex (PDB ID: 2VIY) (29). Refinement was done with PHENIX (30) and Refmac (28), and manual model building was done using O (31) and Coot (32). The final model consists of residues 83–202 and 84–202 of each NS1 ED and residues 429–591 of each β-iSH2 domain. Structure figures were created using PyMol (33).

Cells and Viruses. 293T, A549, 1321N1, and MDCK cells were maintained in Dulbecco's modified Eagle's medium (DMEM) (Invitrogen) supplemented with 10% fetal calf serum at 37 °C with 5% CO_2. MDCK cells stably expressing the V protein of PIV5 (MDCK-V cells) have been described previously (24) and were maintained in the presence of 200 μg/mL G418 (Geneticin; Invitrogen).

A/Udorn/72 wild-type (rUd WT) and mutant viruses were generated by plasmid-based reverse genetics essentially as previously described (16, 34). Briefly, 293T cells were transfected with eight genome-sense (pHH21) plasmids and four protein expression plasmids (pcDNA3.1) encoding PB1, PB2, PA, and NP using FuGENE 6 transfection reagent. At 16 h posttransfection the cells were cocultured with MDCK-V cells in serum-free DMEM containing 2.5 μg/mL N-acetyl trypsin (Sigma). Viruses were propagated through two passages in MDCK-V cells followed by plaque assay titration on MDCK-V cells. Viral RNA was extracted using the QIAamp viral RNA kit, followed by reverse-transcriptase PCR using genome specific primers and the resultant DNA sequenced to confirm presence of the introduced mutations.

Antibodies. Goat serum raised against purified and disrupted A/Udorn/72 virus (anti-Udorn; kindly provided by Robert A. Lamb, Northwestern University, Evanston, IL) was used to detect influenza virus structural proteins by immunoblotting. NS1 was detected using purified sheep antisera (Diagnostics Scotland) raised against the NS1 protein of the A/Puerto Rico/8/34 strain. Myc-tagged β-iSH2, β-actin and pAkt were detected using anti-myc (Upstate Cell Signaling Solutions), anti-β-actin (Sigma-Aldrich) and anti-phospho-Akt (Ser473) (Cell Signaling Technology) monoclonal antibodies, respectively. Immunostaining of plaques was performed using sheep antisera raised against purified and disrupted X31 [H3N2] virus (anti-X31; Diagnostics Scotland).

Immunoblotting. Virus-infected A549 cells were lysed in 2× disruption buffer (6 M urea, 2 M β-mercaptoethanol, 4% sodium dodecyl sulphate) and nucleic acids disrupted by sonication. Samples were boiled for 5 min, polypeptides separated on a NuPAGE 4–12% Bis-Tris gel (Invitrogen) by SDS-PAGE, and transferred to polyvinylidene difluoride membranes (Invitrogen). Membranes were placed in blocking buffer (PBS, 0.1% Tween 20, 5% dried milk) overnight at 4 °C. Membranes were incubated with the appropriate primary antibody and HRP-conjugated secondary antibody in blocking buffer at room temperature for 1 h each, followed by addition of ECL substrate (GE Healthcare) and detection by autoradiography.

GST-Pulldown Experiments. 293T cells transfected with pEF-β-iSH2 were lysed in immunoprecipitation buffer [20 mM Tris-HCl (pH 7.8), 650 mM NaCl, 0.5% NP-40, 5 mM EDTA], sonicated, insoluble material was removed by centrifugation at 13,000 rpm at 4 °C for 10 min, and supernatants were filtered through a 0.45-μm filter. GST-NS1 agarose beads were incubated with the transfected 293T cell lysates overnight at 4 °C. Beads were washed in immunoprecipitation buffer, resuspended in 2× disruption buffer, boiled for 5 min, and proteins were analyzed by SDS-PAGE and immunoblotting.

PIP_3 Assays. Analysis and relative quantification of total PIP_3 levels in 1321N1 cells was performed as previously described (35).

Plaque Assays. MDCK or MDCK-V cells in six-well plates were infected with serial 10-fold dilutions of each virus in serum-free DMEM for 1 h at 37 °C. Cells were overlaid with DMEM-1% agarose supplemented with 2 μg/ml N-acetyl trypsin and incubated at 37 °C for 72 h. Cells were fixed in 5% formaldehyde for 1 h at room temperature, washed in PBS, and blocked in PBN (PBS, 1% BSA, 0.02% sodium azide). Plaques were visualized by immunostaining after incubating the cells with anti-X31 primary antibody diluted in PBN followed by an alkaline phosphatase-conjugated donkey anti-goat secondary antibody (Santa Cruz) diluted in PBN for 1 h each at room temperature. Plaques were visualized using the SIGMA FAST BCIP/NBT substrate (Sigma-Aldrich).

ACKNOWLEDGMENTS. We thank Ian H. Batty (University of Dundee, United Kingdom) for helpful discussions and Robert A. Lamb (Northwestern University, Evanston, IL) for kindly providing the influenza A virus reverse genetics system and goat anti-Udorn serum. This work was supported by the Medical Research Council, United Kingdom (R.E.R. and R.J.R.), and the Scottish Funding Council (R.J.R.). The University of St. Andrews is a charity registered in Scotland (No. SC013532).

1. Cantley LC (2002) The phosphoinositide 3-kinase pathway. *Science*, 296(5573):1655–1657.
2. Manning BD, Cantley LC (2007) AKT/PKB signaling: Navigating downstream. *Cell*, 129(7):1261–1274.
3. McLendon R, et al. (2008) Comprehensive genomic characterization defines human glioblastoma genes and core pathways. *Nature*, 455(7216):1061–1068.
4. Samuels Y, et al. (2004) High frequency of mutations of the PIK3CA gene in human cancers. *Science*, 304(5670):554.
5. Huang CH, et al. (2007) The structure of a human p110alpha/p85alpha complex elucidates the effects of oncogenic PI3Kalpha mutations. *Science*, 318(5857):1744–1748.
6. Miled N, et al. (2007) Mechanism of two classes of cancer mutations in the phosphoinositide 3-kinase catalytic subunit. *Science*, 317(5835):239–242.
7. Mandelker D, et al. (2009) A frequent kinase domain mutation that changes the interaction between PI3Kα and the membrane. *Proc Natl Acad Sci USA*, 106(40):16996–17001.
8. Hale BG, Jackson D, Chen YH, Lamb RA, Randall RE (2006) Influenza A virus NS1 protein binds p85beta and activates phosphatidylinositol-3-kinase signaling. *Proc Natl Acad Sci USA*, 103(38):14194–14199.
9. Li Y, Anderson DH, Liu Q, Zhou Y (2008) Mechanism of influenza A virus NS1 protein interaction with the p85beta, but not the p85alpha, subunit of phosphatidylinositol 3-kinase (PI3K) and up-regulation of PI3K activity. *J Biol Chem*, 283(34):23397–23409.
10. Hale BG, Randall RE, Ortin J, Jackson D (2008) The multifunctional NS1 protein of influenza A viruses. *J Gen Virol*, 89(10):2359–2376.
11. Gallacher M, et al. (2009) Cation currents in human airway epithelial cells induced by infection with influenza A virus. *J Physiol*, 587(13):3159–3173.
12. Ehrhardt C, et al. (2007) Influenza A virus NS1 protein activates the PI3K/Akt pathway to mediate antiapoptotic signaling responses. *J Virol*, 81(7):3058–3067.
13. Zhirnov OP, Klenk HD (2007) Control of apoptosis in influenza virus-infected cells by up-regulation of Akt and p53 signaling. *Apoptosis*, 12(8):1419–1432.
14. Shin YK, et al. (2007) SH3 binding motif 1 in influenza A virus NS1 protein is essential for PI3K/Akt signaling pathway activation. *J Virol*, 81(23):12730–12739.
15. Xing Z, et al. (2009) Differential regulation of antiviral and proinflammatory cytokines and suppression of Fas-mediated apoptosis by NS1 of H9N2 avian influenza virus in chicken macrophages. *J Gen Virol*, 90(5):1109–1118.
16. Jackson D, Killip MJ, Galloway CS, Russell RJ, Randall RE (2009) Loss of function of the influenza A virus NS1 protein promotes apoptosis but this is not due to a failure to activate phosphatidylinositol 3-kinase (PI3K). *Virology*, 396(1):94–105.
17. Bornholdt ZA, Prasad BV (2008) X-ray structure of NS1 from a highly pathogenic H5N1 influenza virus. *Nature*, 456(7224):985–988.
18. Hale BG, Batty IH, Downes CP, Randall RE (2008) Binding of influenza A virus NS1 protein to the inter-SH2 domain of p85 suggests a novel mechanism for phosphoinositide 3-kinase activation. *J Biol Chem*, 283(3):1372–1380.
19. Gack MU, et al. (2009) Influenza A virus NS1 targets the ubiquitin ligase TRIM25 to evade recognition by the host viral RNA sensor RIG-I. *Cell Host Microbe*, 5(5):439–449.
20. Hale BG, Barclay WS, Randall RE, Russell RJ (2008) Structure of an avian influenza A virus NS1 protein effector domain. *Virology*, 378(1):1–5.
21. Bornholdt ZA, Prasad BV (2006) X-ray structure of influenza virus NS1 effector domain. *Nat Struct Mol Biol*, 13(6):559–560.
22. Das K, et al. (2008) Structural basis for suppression of a host antiviral response by influenza A virus. *Proc Natl Acad Sci USA*, 105(35):13093–13098.
23. Zeqiraj E, Filippi BM, Deak M, Alessi DR, van Aalten DM (2009) Structure of the LKB1-STRAD-MO25 Complex Reveals an Allosteric Mechanism of Kinase Activation. *Science*, 326(5960):1707–1711.
24. Andrejeva J, Young DF, Goodbourn S, Randall RE (2002) Degradation of STAT1 and STAT2 by the V proteins of simian virus 5 and human parainfluenza virus type 2, respectively: Consequences for virus replication in the presence of alpha/beta and gamma interferons. *J Virol*, 76(5):2159–2167.
25. Hilton L, et al. (2006) The NPro product of bovine viral diarrhea virus inhibits DNA binding by interferon regulatory factor 3 and targets it for proteasomal degradation. *J Virol*, 80(23):11723–11732.
26. Min JY, Li S, Sen GC, Krug RM (2007) A site on the influenza A virus NS1 protein mediates both inhibition of PKR activation and temporal regulation of viral RNA synthesis. *Virology*, 363(1):236–243.
27. Frangioni JV, Neel BG (1993) Solubilization and purification of enzymatically active glutathione S-transferase (pGEX) fusion proteins. *Anal Biochem*, 210(1):179–187.
28. CCP4 (1994) The CCP4 suite: Programs for protein crystallography. *Acta Crystallogr D*, 50:760–763.
29. McCoy AJ, et al. (2007) Phaser crystallographic software. *J Appl Crystallogr*, 40:658–674.
30. Adams PD, et al. (2002) PHENIX: Building new software for automated crystallographic structure determination. *Acta Crystallogr D*, 58(11):1948–1954.
31. Jones TA, Zou JY, Cowan SW, Kjeldgaard M (1991) Improved methods for building protein models in electron density maps and the location of errors in these models. *Acta Crystallogr A*, 47(2):110–119.
32. Emsley P, Cowtan K (2004) Coot: Model-building tools for molecular graphics. *Acta Crystallogr D*, 60(12):2126–2132.
33. DeLano WL (2002) *The PyMOL Molecular Graphics System* (DeLano Scientific, Palo Alto, CA).
34. Fodor E, et al. (1999) Rescue of influenza A virus from recombinant DNA. *J Virol*, 73(11):9679–9682.
35. Gray A, Olsson H, Batty IH, Priganica L, Downes CP (2003) Nonradioactive methods for the assay of phosphoinositide 3-kinases and phosphoinositide phosphatases and selective detection of signaling lipids in cell and tissue extracts. *Anal Biochem*, 313(2):234–245.
36. Xia S, Monzingo AF, Robertus JD (2009) Structure of NS1A effector domain from the influenza A/Udorn/72 virus. *Acta Crystallogr D*, 65(1):11–17.
37. Orchiston EA, et al. (2004) PTEN M-CBR3, a versatile and selective regulator of inositol 1,3,4,5,6-pentakisphosphate (Ins(1,3,4,5,6)P5). Evidence for Ins(1,3,4,5,6)P5 as a proliferative signal. *J Biol Chem*, 279(2):1116–1122.